

Visual Whole-Body Control for Legged Loco-Manipulation

Minghuan Liu^{*1,2}, Zixuan Chen^{*1,3}, Xuxin Cheng¹, Yandong Ji¹, Rizhao Qiu¹, Ruihan Yang¹, Xiaolong Wang¹

¹UC San Diego, ² Shanghai Jiao Tong University, ³ Fudan University

<https://wholebody-bl.github.io>

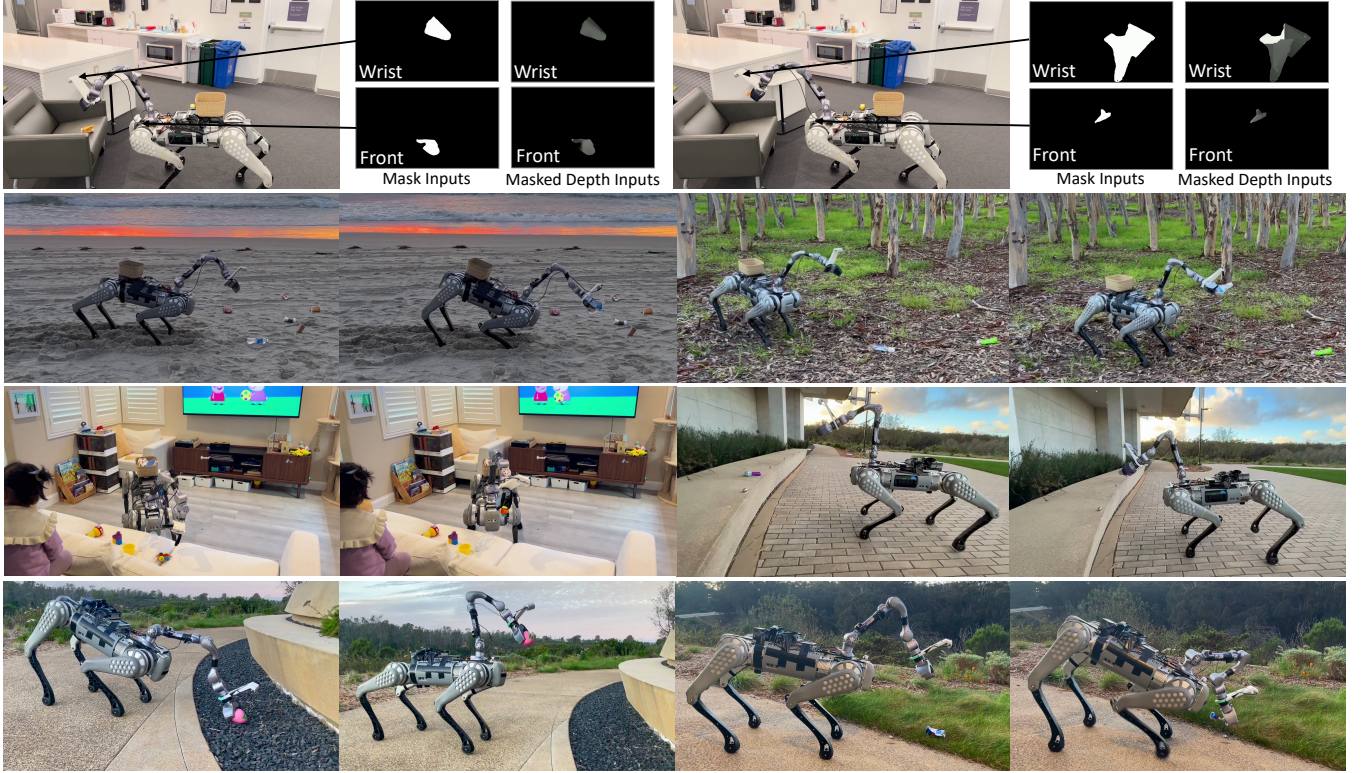


Fig. 1: **Real-Robot input visualization and grasping trajectory.** Our framework enables the robot to grasp different objects in varying heights and surroundings. Our policy is trained in simulation using visual inputs (masks and masked depth images from two views) and can be deployed in real robots without any real-world fine-tuning.

Abstract—We study the problem of mobile manipulation using legged robots equipped with an arm, namely legged loco-manipulation. The robot legs, while usually utilized for mobility, offer an opportunity to amplify the manipulation capabilities by conducting whole-body control. That is, the robot can control the legs and the arm at the same time to extend its workspace. We propose a framework that can conduct the whole-body control autonomously with visual observations. Our approach, namely Visual Whole-Body Control (VBC), is composed of a low-level policy using all degrees of freedom to track the body velocities along with the end-effector position, and a high-level policy proposing the velocities and end-effector position based on visual inputs. We train both levels of policies in simulation and perform Sim2Real transfer for real robot deployment. We perform extensive experiments and show significant improvements over baselines in picking up diverse objects in different configurations (heights, locations, orientations) and environments.

* The first two authors contributed equally.

I. INTRODUCTION

The study of mobile manipulation has achieved large advancements with the progress of better manipulation controllers and navigation systems. While installing wheels for a manipulator can help solve most household tasks [75, 23], it is very challenging to adopt these robots outdoors with challenging terrains. Imagine going camping; having a robot picking up trash and wood for us would be very helpful. To achieve such flexibility and applications in the wild, we study mobile manipulation with legged robots equipped with an arm, i.e., legged loco-manipulation. Specifically, we are interested in how the robot can conduct tasks based on its visual observation autonomously.

An important aspect of loco-manipulation is the opportunity to conduct whole-body control using all degrees of freedom

of the robot. While the legs are typically utilized for mobility, there is a large potential for controlling all the joints of the legs and arms together to amplify manipulation capabilities. We humans do this, too: We use our legs to stand up to reach a book placed on a shelf; We bend our legs to tie our shoes. Fig. 1 shows the tasks our robot can do when controlling the whole-body joints together. For example, our robot can go to the side of the road and pick up the trash on the grass. This will be unachievable without bending the front legs of the robot. The arm alone will not be long enough to reach the ground.

While this is appealing, it is a very challenging control problem to coordinate all the joints simultaneously with large degrees of freedom (19 DoF). The robot will need to exploit the contact with its surroundings and the objects and maintain stability and robustness to external disturbances all at the same time. Besides, acquiring a mobile robot platform to do precise manipulation jobs requires a steady robot body, which is much harder for legged robots compared to wheeled robots. An even larger challenge comes from achieving all these in diverse environments autonomously, given only the observation from an egocentric camera. Recent learning-based approaches have shown promising results on legged robots avoiding obstacles, climbing stairs, and jumping over stages robustly with visual inputs [13, 1, 82, 15]. However, all these efforts still focus only on locomotion without manipulation, which requires more precise control. The extra complexity and more challenging tasks make direct end-to-end learning infeasible.

In this paper, we conduct loco-manipulation by introducing a two-level framework with a high-level policy proposing end-effector pose and robot body velocity commands based on visual observations and a low-level policy tracking these commands. Such a hierarchical design is effective as the low-level controller can be effectively shared when interacting with diverse environments and objects. We named our framework **Visual Whole-Body Control (VBC)**. Specifically, VBC is a hierarchical solution that contains three stages of training: first, we train a universal low-level policy using reinforcement learning (RL) to track any given goals and achieve whole-body behaviors; then, we train a privileged teacher policy by RL to provide a set of appropriate goals and guide the low-level policy to accomplish specific tasks (e.g., pick-up); finally, to deploy the policy into the real robot, we distill the teacher policy into a depth-image-based visuomotor student policy via online imitation learning. All this training is done in simulation, and we perform direct Sim2Real transfer for deployment in the real robot.

Our hardware platform is built on a Unitree B1 quadruped robot equipped with a Unitree Z1 robotic arm. We design a server-client multi-processing system that consists of four different modules working under different frequencies. We conducted the pickup task with 14 different objects, including regular shapes, daily uses, and irregular objects, under three height configurations, i.e., on the ground, on a box, and on a table, achieving a high success rate in all scenarios.

We summarize the contribution of this paper as:

- We develop an autonomous vision-based loco-

manipulation system that utilizes model-free RL and sim-to-real techniques to learn whole-body control policies for legged robots.

- Our proposed method emerges retrying behavior and generalizes well to complicated terrains, various objects, and heights.

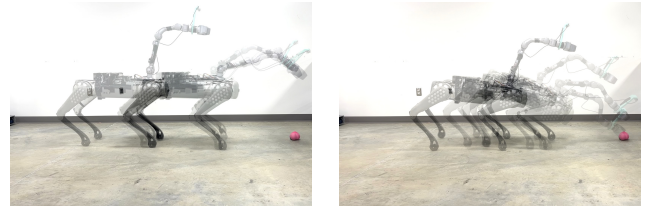
II. RELATED WORK

Legged Locomotion. For decades, legged locomotion has been an essential topic in the field of robotics and has gained much success. Classical methods solve the legged locomotion task through model-based control to define controllers in advance. For example, Miura and Shimoyama [50], Sreenath et al. [61] utilized traditional methods to enable the walking of biped robots. MIT cheetah 3 [7], ANYmal-a [31] by ETH, and Atlas [19] by Boston Dynamics are good examples of robots designed with a robust walking controller. Based on these developed robots, researchers have been able to develop advanced controllers for even more agile locomotion tasks, such as jumping or walking over varying obstacles [53, 51, 26, 52, 3, 38]. To make a robust controller that can adapt to varying environments, researchers integrate some sensor data such as elevation maps [18, 40, 35, 6, 17] and state estimators [8, 66, 10, 74, 65]. Although classical methods have greatly succeeded in legged locomotion, generalizability in pre-designed controllers would require careful and tedious engineering efforts. With the fast development of deep neural networks, learning-based end-to-end methods have become a simple way to gain robust controllers with strong generalization abilities. Learning-based methods often train a robust controller in physics simulators such as PyBullet [14] and Isaac Gym [47] and then perform sim-to-real transfer to a real robot. For example, Rudin et al. [58] uses Isaac Gym with GPU to enable a quadruped robot to walk in only several minutes, Kumar et al. [36, 37] proposed the RMA algorithm to make the sim-to-real transfer process easier, and more robust, Lee et al. [41], Miki et al. [49], Agarwal et al. [1], Yang et al. [73], Yu et al. [80], Cheng et al. [13], Zhuang et al. [82], Fu et al. [21], Margolis and Agrawal [48], Li et al. [44] enable the legged robots to walk or run on varying terrains, and Fuchioka et al. [24], Escontrela et al. [16], Peng et al. [54], Yang et al. [71], Wang et al. [64], Li et al. [43], Kumar et al. [39] combine RL with imitation learning to produce naturalistic and robust controllers for legged robots. Kim et al. [33] map human motions to a quadruped robot to complete a wide range of locomotion and manipulation tasks.

Mobile Manipulation. Previously mentioned works mainly focus only on the mobility part; adding manipulation to the mobile base is yet to be well-solved. Autonomous mobile manipulation on wheeled robot platforms has made significant progress over the past few years. Wong et al. [68] collected teleoperated mobile manipulation data and learned imitation-learning-based policies in simulation. Lew et al. [42] built an efficient framework for table cleaning with RL and trajectory optimization. Garrett et al. [25] and Srivastava et al. [62] integrate task-specific planner for various mobile manipulation

tasks. Gu et al. [27] and Xia et al. [69] developed modularized mobile manipulators with RL, Yokoyama et al. [78] introduced a high-level controller for coordinating different low-level skills. Sun et al. [63] designed a modularized policy with components for manipulation and navigation, trained by RL to learn navigation and grasping indoors. Yang et al. [72] proposed simultaneously controlling the robot arm and base for harmonic mobile manipulation using RL training with large-scale environments. Ahn et al. [2] pre-trained a set of single mobile or manipulation tasks and relied on large language models to decompose and call the skills to achieve long-horizon tasks. Brohan et al. [9] train a robotics transformer to perform real-world tasks given human instructions, trained on large-scale and real-world demonstration. Shafiullah et al. [59] learned to solve household tasks from 5-minute demonstrations based on pre-trained home representations. While encouraging, most of these mobile manipulators with wheels cannot operate with challenging terrains in the wild.

Legged Loco-Manipulation A set of works has exploited legged loco-manipulation to take advantage of legged robots. Bellicoso et al. [5] designs an online motion planning framework, together with a whole-body controller based on a hierarchical optimization algorithm to achieve loco-manipulation, Fu et al. [22] proposed an effective method to train a whole-body controller end-to-end through DRL. Ma et al. [46] combined model-based manipulator control and learning-based locomotion, but only showed the response to external push instead of achieving manipulation tasks. Notably, these works all require human involvement and teleoperation to execute and achieve tasks, rather than operating autonomously. Zhang et al. [81], Yokoyama et al. [79], Arcari et al. [4] all performed an autonomous mobile manipulation system on quadruped robots while they utilized the default model-based controller provided through the robot APIs (only control robot locomotion in a static height) and only focused on the manipulation part without any whole-body behaviors to adapt to different heights of objects. Ferrolho et al. [20] proposed a trajectory optimization framework based on a robustness metric for solving complex loco-manipulation tasks, but the task is assigned and the target positions are calculated via a motion capture system, thus only works in limit. Sleiman et al. [60] realized a bilevel search strategy for motion planning, by incorporating domain-specific rules, combining trajectory optimization, informed graph search, and sampling-based planning, enabling robots to perform complex tasks. They require the user to provide a dense description of the scene to initialize the solver. Zimmermann et al. [83] also utilized trajectory optimization to enable a legged robot to walk and pick up objects. However, they only show limited surroundings and simple objects. Besides these works with arm-based configuration, Wolfslag et al. [67] use the legs for pushing and box lifting tasks by introducing additional support legs named prongs to enhance the robustness and manipulation capabilities of quadrupedal robots. Jeon et al. [32] adopted a similar hierarchical framework to us, but does not involve any visual inputs, and only learned a quadruped for pushing large objects without an additional arm.



(a) Non-whole-body method. (b) VBC (ours).

Fig. 2: Illustration of comparing VBC to non-whole-body method. The robot body of the non-whole-body method does not bend to allow the arm to reach the objects on the ground.

The system we design highly differs from the aforementioned works, as our work is a fully *autonomous* and vision-based mobile manipulation system on quadruped robots, with limited human intervention. The robot is controlled and planned by an end-to-end policy integrated with perception and control, able to adapt to objects with varying heights through its whole-body behavior, and emerges retrying behaviors when the task fails. Due to our design of visual inputs, our system can work both indoors and outdoors with no external limits, as illustrated in Fig. 1, compared with almost all of the above-mentioned works that are only tested in limited lab scenarios. In Fig. 2 we show why VBC is highly advantaged of the non-whole-body methods [81, 79, 4], for the body control behavior allowing much more flexible poses (e.g., bending) to reach objects in random heights, like the one on the ground.

III. VISUAL WHOLE-BODY CONTROL

In this section, we introduce our Visual Whole-Body Control (VBC) framework (as described in Fig. 3). Our VBC framework consists of a low-level goal-reaching policy and a high-level task-planning policy. Our low-level goal-reaching policy tracks a root velocity command and a target end-effector pose. Our vision-based high-level task-planning policy provides velocity and end-effector pose command to the low-level policy, given the segmented depth images and proprioception of the robot as inputs. When combined, our robot could operate fully autonomously using only visual input and its proprioception. We start with an overview of our robot setup, followed by the training pipeline of the low-level policy and the high-level policy, and our robot system design.

A. Robot Platform Overview

The robot platform used in this work comprises a Unitree B1 quadruped robot with a Unitree Z1 robot arm and a gripper mounted on its back. Our robot is equipped with two cameras, one on the head and another mounted close to the gripper. The Unitree B1 quadruped has 12 actuatable DoFs, the arm has 6 DoFs, and the gripper has another 1 DoF, so there are 19 DoFs in total. An overview of the hardware setup is shown in Fig. 4.

B. Low-Level Policy for Whole-Body Goal-Reaching

The low-level control policy that takes over the whole-body locomotion control π^{low} as described in the blue part

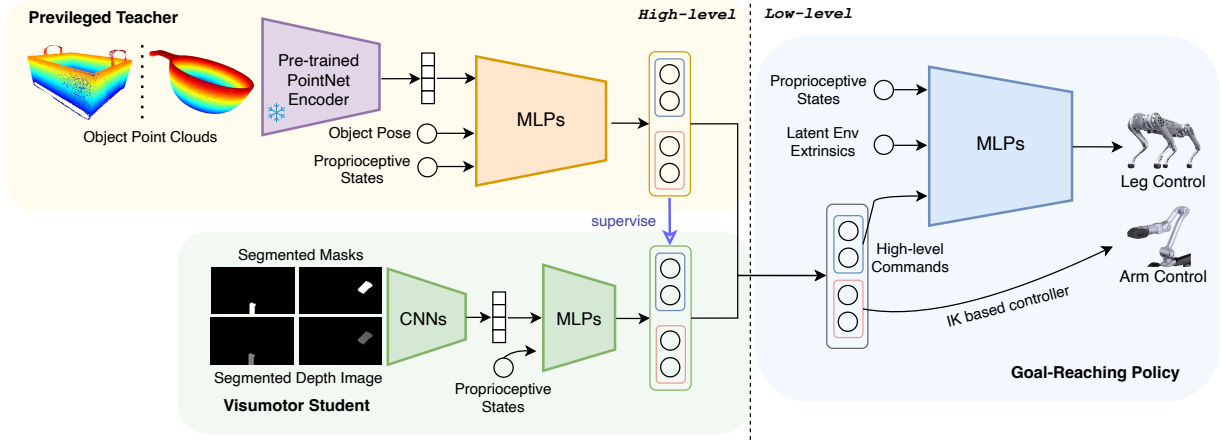


Fig. 3: **Training a vision-based whole-body policy for loco-manipulation.** Our VBC framework trains a low-level control policy and a high-level planning policy using reinforcement learning and imitation learning.

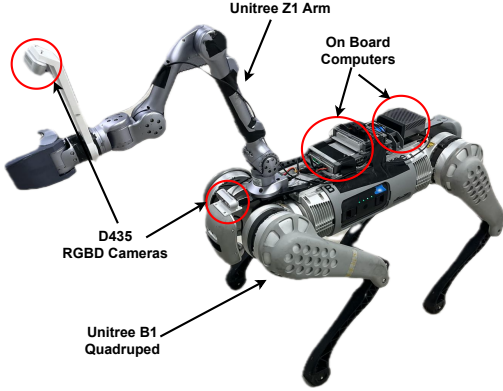


Fig. 4: **Real robot system setup.**

in Fig. 3, is trained to track any given end-effector poses and body velocities across various terrains. In this work, we turn to the help of RL and utilize ROA (Regularized Online Adaptation) [22, 12, 32] to realize such a universal and robust behavior that can become the foundation of any high-level tasks.

Commands. The command \mathbf{b}_t for our low-level policy is defined as:

$$\mathbf{b}_t = [\mathbf{p}^{\text{cmd}}, \mathbf{o}^{\text{cmd}}, v_{\text{lin}}^{\text{cmd}}, \omega_{\text{yaw}}^{\text{cmd}}]$$

where $\mathbf{p}^{\text{cmd}} \in \mathbb{R}^3$, $\mathbf{o}^{\text{cmd}} \in \mathbb{R}^3$ are end-effector position and orientation¹ command; $v_{\text{lin}}^{\text{cmd}} \in \mathbb{R}$, $\omega_{\text{yaw}}^{\text{cmd}} \in \mathbb{R}$ are the desired forward linear and angular velocity, respectively. During the low-level policy training, we uniformly sample the linear velocity from the range $[-0.6\text{m/s}, 0.6\text{m/s}]$ and robot yaw velocity from $[-1.0\text{m/s}, 1.0\text{m/s}]$. When solving downstream tasks, the commands are specified by our high-level task-planning policy and further clipped into smaller ranges.

Observations. The observation of our policy is defined as a 90-dimensional vector \mathbf{o}_t :

$$\mathbf{o}_t = [\mathbf{s}_t^{\text{base}}, \mathbf{s}_t^{\text{arm}}, \mathbf{s}_t^{\text{leg}}, \mathbf{a}_{t-1}, \mathbf{z}_t, \mathbf{t}_t, \mathbf{b}_t].$$

¹We use Euler angle parameterization by default in this paper.

Among them, $\mathbf{s}_t^{\text{base}} \in \mathbb{R}^5$ is the current quadruped base state including (row, pitch, and quadruped base angular velocities), $\mathbf{s}_t^{\text{arm}} \in \mathbb{R}^{12}$ is arm state (position and velocity of each arm joint except the end-effector), $\mathbf{s}_t^{\text{leg}} \in \mathbb{R}^{28}$ is leg state (joint position and velocity of each leg joint, and foot contact patterns that are 0 or 1), $\mathbf{a}_{t-1} \in \mathbb{R}^{12}$ is the last output of policy network, $\mathbf{z}_t \in \mathbb{R}^{20}$ is environment extrinsic vector, which is an encoding of environment physics. Besides, following the work of [1], to learn a steady walking behavior (like trotting), we provide some extra timing reference variables \mathbf{t}_t to the observation, which is computed from the offset timings of each foot by repeat the gait cycle of the desired symmetric quadrupedal contact pattern.

Actions. Our low-level goal-reaching policy controls the quadruped robot and the mounted arm simultaneously. For the quadruped robot, our low-level policy outputs the target joint angles for all 12 joints of the robot, which is converted to torque command by a PD controller.

Arm control. Previous work [22] has revealed that whole-body RL policy is good at controlling the end-effector position but struggles in controlling the end-effector orientation. Unfortunately, such behaviors are critical for our manipulation tasks. Thereafter, we solve the inverse kinematic (IK) with the pseudoinverse Jacobian method² to convert the end-effector pose command into target joint angles for controlling the arm. Formally, IK computes the increment of the current joint position $\Delta\theta \in \mathbb{R}^6$

$$\Delta\theta = J^T (JJ^T)^{-1} \mathbf{e}, \quad (1)$$

where J is the Jacobian matrix, and $\mathbf{e} \in \mathbb{R}^6$ is the difference between the current end-effector pose and the next end-effector pose represented as the position and the Euler angle.

Reward function. Our reward for training the low-level policy for whole-body control mainly consists of four parts:

²More advanced IK solver can be exploited for better performance under certain circumstances, but the pseudoinverse Jacobian method works well enough for the problem studied in this paper.

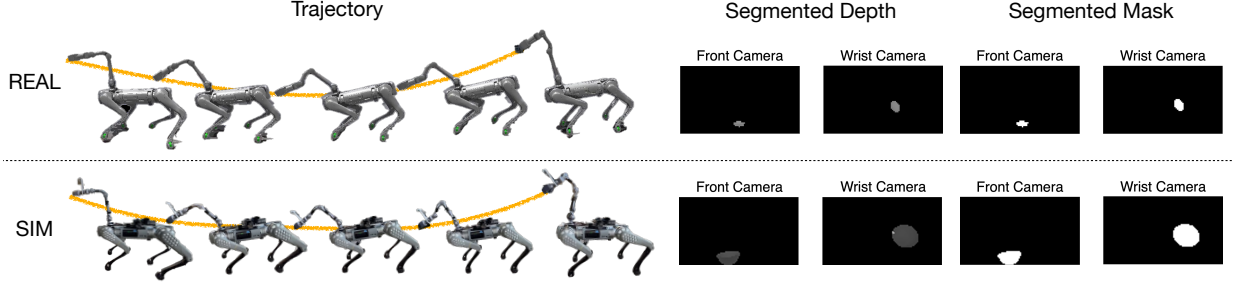


Fig. 5: **Comparison between trajectories and segmented depth images in simulation and real-world sampled by VBC.** Left: The real-world behaviors match great with the simulation, indicating a less sim-to-real gap in our method. Right: Our TrackingSAM-based working pipeline allows us to obtain the segmentation mask precisely during deployment (not the same object observed). The depth images are pre-processed by hole-filling and clipping.

command-following reward, energy reward, alive reward, and phase reward. The command following reward encourages the robot to track and follow the provided commands and explore various whole-body behaviors; the energy reward penalizes energy consumption to enable smooth and reasonable motion; the alive reward encourages the robot not to fail; the phase reward encourages the robot to walk in a steady behavior as mentioned above.

End-effector goal poses sampling. To train a robust low-level controller for goal-reaching, we sample and track various gripper poses. For sampling smooth trajectories of gripper target poses for tracking, we employ a height-invariant coordinate system originating at the robot’s base and randomly sample trajectories on this at every fixed timestep. This ensures the sampled trajectories are always on a smooth sphere and prevents the sampled goals from being affected by the quadruped robot’s height. Details can be found in Appendix II-A.

Policy architecture. The low-level control policy network is a three-layer MLP, where each layer has 128 dimensions and ELU activations. It receives observations, including the extrinsic latent environment, which is encoded by the privileged encoder during training, and the adaptation module during testing. The privileged information encoder that models environment physics parameters is a two-layer MLP with a hidden size of 64; the adaptation module encodes history rollouts, which is a two-layer convolutional network.

Domain randomization. When training, we randomize the type of terrains, including flat plane and rough ones. We also randomized the friction between robots and terrains. Besides, we randomized the quadruped’s mass and center of mass. These randomizations, together with our ROA module, contribute to a robust low-level policy.

C. High-Level Policy for Task Planning

When deploying our policy into the real world, the robot can only perceive the object through depth images to achieve high-frequency control. However, RL with visual observation is quite challenging and requires particular techniques to be efficient [30, 77, 29, 28, 70]. To achieve simple and stable training, we choose to train a privileged state-based policy that

can access the shape information of the object (as described in the orange part of Fig. 3) and distill a visuomotor student (as described in the green part of Fig. 3).

C.1. Privileged Teacher Policy

Like the low-level policy, the privileged teacher policy is trained through RL (we also use PPO in this work) with designed task-specific reward functions and domain randomization, with a fixed low-level policy underlying.

Privileged observations. The privileged observations include the encoded shape feature and object poses. We formally define it as a 1094-dim vector:

$$\mathbf{o}_t = [\mathbf{z}^{\text{shape}}, \mathbf{s}_t^{\text{obj}}, \mathbf{s}_t^{\text{proprio}}, \mathbf{v}_t^{\text{base vel}}, \mathbf{a}_{t-1}],$$

where $\mathbf{z}^{\text{shape}} \in \mathbb{R}^{1024}$ is the latent shape feature vector encoded from the object point clouds using a pre-trained PointNet++ [55]. The pre-trained PointNet++ is fixed, so $\mathbf{z}^{\text{shape}}$ remains invariant during training. $\mathbf{s}_t^{\text{obj}} \in \mathbb{R}^6$ is the object pose in local observation w.r.t the robot arm base. It contains the local pose of the object. The use of local coordination inherently incorporates the information regarding the distance to the object. $\mathbf{s}_t^{\text{proprio}} \in \mathbb{R}^{53}$ consists of joint positions including gripper joint position $\mathbf{q}_t \in \mathbb{R}^{19}$, joint velocity not including gripper joint velocity $\dot{\mathbf{q}}_t \in \mathbb{R}^{18}$, and end-effector position and orientation $\mathbf{s}_t^{\text{ee}} \in \mathbb{R}^6$. $\mathbf{v}_t^{\text{base vel}} \in \mathbb{R}^3$ is the base velocity of robot and $\mathbf{a}_{t-1} \in \mathbb{R}^9$ is the last high-level action.

High-level Actions. The high-level policy π^{high} outputs actions that determine the velocities and the target end-effector position for the low-level policy. The high-level action is formally defined as:

$$\mathbf{a}_t = [\mathbf{p}_t^{\text{cmd}}, \mathbf{v}_t^{\text{cmd}}, p_t^{\text{grripper}}] \in \mathbb{R}^9,$$

where $\mathbf{p}_t^{\text{cmd}} \in \mathbb{R}^6$ is the increment of gripper pose, $\mathbf{v}_t^{\text{cmd}} \in \mathbb{R}^2$ is the command of quadruped linear velocity and yaw velocity and $p_t^{\text{grripper}} \in \{0, 1\}$ indicates the gripper status (close or open).

Reward functions. The reward function for training our state-based policy comprises stage rewards and assistant rewards, as defined in Tab. III. As for the task-specific rewards, we design three stages. The first stage is approaching, and the

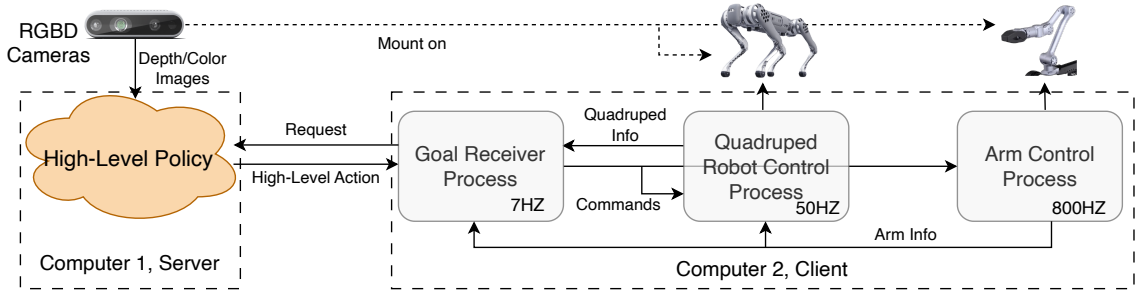


Fig. 6: **The server-client multi-processing system design.** Modules work asynchronously under different frequencies. The high-level planning policy (left) and the low-level control modules (right, controlling arm and legs) are deployed on different devices. To be more specific, the goal receiver requests the high-level policy to take the visual input and receive the new commands; the low-level policy sends joint position commands to the quadruped runs at 50Hz, given the input of high-level commands; the IK-based arm controller runs and send the joint position command to the arm constantly at 800Hz, given the target end-effector pose. Therefore, the low-level policy and the arm controller keep utilizing the old commands to control the robot until the high-level policy updates the commands (i.e., target robot velocities and end-effector pose).

corresponding reward r_{approach} encourages the gripper and quadruped to get close to the target object:

$$r_{\text{approach}} = \min(d_{\text{closest}} - d, 0), \quad (2)$$

where d_{closest} is the current minimum distance between the gripper and the target object. The second stage is task progress, and the reward r_{progress} leads the robot to the desired final state, e.g., lifting the object in the pickup task:

$$r_{\text{progress}}^{\text{pickup}} = \min(d - d_{\text{highest}}, 0), \quad (3)$$

where d_{highest} is the current largest height of the object. The third stage is denoted task completion, and reward $r_{\text{completion}}$ bonus when the agent completes the task.

$$r_{\text{completion}} = 1(\text{Task is completed}), \quad (4)$$

For example, in the pickup task, the task completion condition is that the object height exceeds the required threshold. Note that at one time, the robot can only be at one stage and receive one stage reward of the above three, ensuring that different task stages are not intervened in. The assistant rewards are designed to a) smooth the robot’s behavior to be easier to transfer to the real world, like penalty huge action commands and joint acceleration; b) prevent deviation and sampling useless data, such as acquiring the robot’s body and gripper to point to the object, which guarantees that the camera does not lose tracking objects. Beyond these major rewards, we also design a set of assistant reward functions that help accelerate the learning procedure, see details in Appendix II-B.

Domain randomization. When training our high-level policy, we randomized the friction between the robot and the terrain, the mass of the robot, and the center of mass of the robot. Although our low-level control policy can handle these gaps in the real world, its performances differ under different environmental conditions. These randomizations help the high-level policy adjust better to different low-level performances. Moreover, due to the uncertainty of the high-low signal transmission in the real world, we also randomize the high-level frequency

by involving different low-level policy calls during one high-level call. We also randomize the Kp and Kd parameters for the arm controller as we use the built-in position control mode for the arm in the simulation. Regarding the pick-up task, we randomize table heights, the initial position and pose of the robot, along with the position and pose of objects.

C.2. Visuomotor Student Policy We find robust and adaptive picking-up behaviors emerge from the privileged teacher policy training, with inaccessible object poses and shape features in reality. To deploy our policy in the real world, we must use easily accessible real-world observations like images.

Observations and actions. Although camera images are easily accessible both in simulation and the real world, there is a huge gap for colored images between the simulation and the real world. This persuades us to use depth images only. To further decrease the noise and gap from backgrounds, we use the segmented depth images and also their segmentation masks. Formally, the observation of our vision policy is

$$\mathbf{o}_t = [\mathbf{o}_t^{\text{image}}, \mathbf{s}_t^{\text{proprio}}, \mathbf{a}_{t-1}],$$

where $\mathbf{o}_t^{\text{image}}$ consists of object segmentation masks and segmented depth images. $\mathbf{s}_{\text{proprio}}$ and \mathbf{a}_{t-1} are proprioceptive observation and last action defined above. The output actions are the same as those of state-based policy.

Imitation learning for student distillation. To deploy our policy in the real world, we distill our state-based high-level planning policy into a vision-based policy using DAgger. We warm up by teacher sampling the initial transition data. This is like behavior cloning (BC) to find a good initialization of the visuomotor student policy to improve the training efficiency. Then we sample transitions using the student policy and request correction from the teacher. We find this is much more efficient and effective than directly learning a visuomotor student policy using RL. We adopt augmentations like RandomErasing, GaussianBlur, GaussianNoise, and RandomRotation for the depth images. More details can be found in Appendix II-B.



Fig. 7: **Segmented examples of the TrackingSAM tool.** At the beginning of each reset trial, we annotated the objects from the two RGBD cameras mounted on the gripper and the robot head. Then, TrackingSAM will keep tracking the segmented object and providing the mask.

Policy network architecture. Our vision-based high-level policy network comprises a CNN and a two-layer MLP that outputs the high-level actions. We concatenate the images and other states as observations. We stack 4-step images which are passed through the two-layer CNN network with kernel size being 5 and 3, respectively, and then encoded as a 64-dim latent vector. Then, we concatenate this latent vector with other states as a flattened vector. This vector is then passed to a two-layer MLP with a hidden size of 64. We use ELU as the activation.

D. Real World Deployment

Hardware setup. As visualized in Fig. 4, we mount two cameras on our robot platform, which are both RealSense D435 cameras. B1 itself has an onboard computer, and we also attached an additional onboard computer, Nvidia Jetson Orin, to the robot. The B1, Z1, and the Orin computer are all powered by B1’s onboard battery. The inference of the low-level policy and the control of the arm is conducted at the onboard computer of B1, and that of the high-level vision-based planning policy is made on Nvidia Jetson Orin. It is worth noting that the computation and the power of our robot system are fully onboard and, therefore, untethered.

System design. During deployment, the low-level policy that controls the quadruped works at a frequency of 50Hz; in the meantime, the high-level policy runs at 8Hz, which is five times slower than the low-level policy; besides, the arm is required to work at a frequency of more than 800Hz. Since these policies work on different computers, along with the quadruped and the arm should work under different frequencies, we design a client-server multi-processing system for this work, as shown in Fig. 6. We set up three processes at the low-level policy side: a quadruped robot control process, an arm control process, and a goal receiver process behaving as a client. The high-level policy combines the vision inputs from the depth cameras and the information from the low-level request as the observation works as a server. Every 0.1 seconds, the goal receiver sends a request with the necessary information to the server; the high-level policy makes the latest inference and sends the high-level action back to the robot; at the same time, the quadruped and the arm control processes gather the latest high-level commands to execute,

while keep updating the necessary information for the goal receiver process.

Sim-to-real transfer. We made several efforts to bridge the sim-and-real gap. Specifically, we slightly randomize the position and rotation of both our cameras to enable our policy to handle slight camera offsets from simulation. Besides, we clip the depth image to a minimum of 0.2m to avoid low-quality images when the distance is too close to a real camera, after which we normalize the depth value. As the surrounding environment in the simulation and the real world are very different, to reduce the noise, we only use segmented depth images to train our visuomotor policy.

Vision masks. Note that our system works with only limited human intervention, i.e., we need to annotate and segment objects from environment backgrounds. To this end, we develop TrackingSAM [56], a tool that combines the tracking model AOT (Associating Objects with Transformers) [76] and SAM (Segment Anything) [34]. This allows us to annotate the object on the image from both cameras or an arbitrary image before starting the task and track that object to provide its real-time segmented masks. The tool is integrated into the high-level server, and a demo example can be found in Fig. 7. During real-world experiments, we annotated the objects from the two RGBD cameras mounted on the gripper and the robot head at the beginning of each reset trial. TrackingSAM will keep tracking the segmented object and providing the mask. The depth images obtained from the RGBD cameras are pre-processed by hole-filling and clipping. In real-world experiments, as long as the object is visible to one camera (either the head or the wrist camera), the annotation mask can be propagated to both views to initialize an automated pickup.

IV. EXPERIMENTS

We conduct a set of experiments on pick-up tasks to compare VBC with baselines both in simulation and the real world, showing effectiveness from the following perspectives:

- VBC solves the mobile manipulation (pickup) task over varying objects with different heights;
- VBC has the advantage over easy baseline methods, such as decoupling mobile manipulation problems into separate moving and arm-control;
- The object shape feature produced by pre-trained PointNet++ boosts learned policy grasp varying objects;

Experiment setups. The simulation / real-world setup is shown in Fig. 8. Particularly, in the simulation, the high-level policy is trained to pick up various objects on a range of table heights [0, 0.65] meter. We utilize IsaacGym [47] for parallel training in a large set of environments. In the real world, we initialize objects in a random location and orientation, and put them in front of the robot where it is visible through both cameras (around 0.5~1.5m). We test three different heights by putting the objects on the ground, on a box, and on a table, corresponding to the heights of 0.0m, around 0.3m, 0.5m.

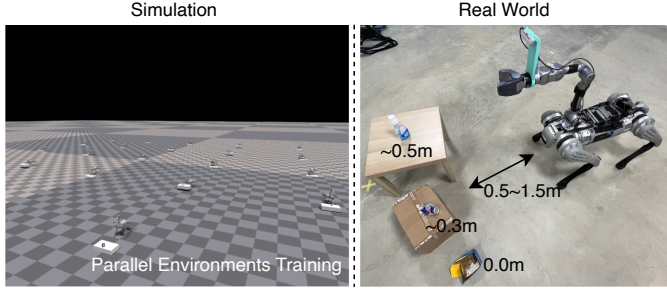


Fig. 8: **Illustration of simulation / real-world setup.**

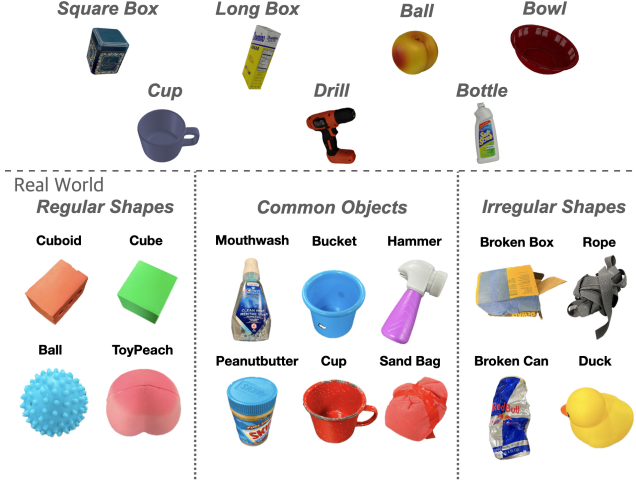


Fig. 9: **Examples of training objects and real-world objects.**

A. Simulation Results

Objects. The objects used for the benchmark problems are shown in Fig. 9. Specifically, we included 34 objects in total, mainly adapted from the YCB dataset [11]. According to the object shapes, we roughly divided them into 7 categories: *ball*, *long box*, *square box*, *bottle*, *cup*, *bowl* and *drill*.

Evaluation principles and baselines. In the simulation, when the environment is reset and a new trail begins, both the robot and the objects are initialized with random positions and poses, and it’s considered a success if an object is picked up and a failure when the object falls down the table or is not successful in 150 high-level steps. During experiments, we compare both the privileged teacher policies of VBC against baselines, and their visuomotor student policies over 34 kinds of different objects: 1) VBC w.o. shape feature: a visuomotor policy that is trained the same as VBC, but does not access the pre-trained object shape features during the teacher training stage. This aims to show the necessity of the object shape features during teacher training. We only compare the teacher’s performance as the only difference comes from the teacher’s side. 2) Floating base: a floating base policy with a perfect low-level navigation ability but without whole-body behavior; in other words, the robot can always follow the given velocity commands and body height commands ranging from 0.4 to 0.55 meters (we set 0.4 meters as the lower bound as

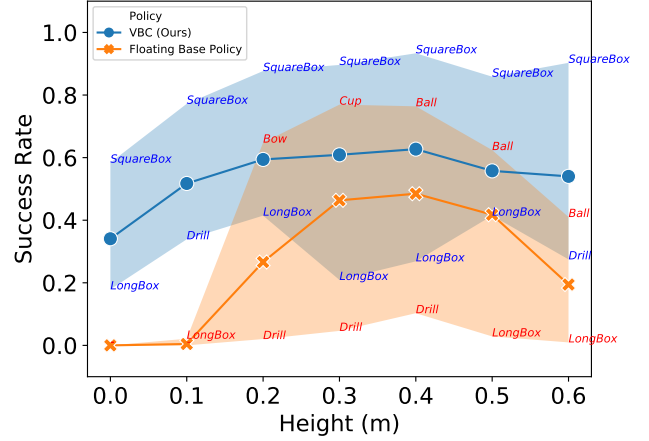


Fig. 10: **Success rates** of different student policies at different heights, tested in the *simulator*. Each distinct object for more than 100 episodes. The robot starts from a 1.0-meter distance from the table. Every episode ends when the robot successfully picks up the object, the object falls from the table, or the robot fails until 150 steps (~ 18 seconds). The dots represent the *mean* performance of all objects, and the upper and the lower bound represent the maximum and the minimum success rate overall 7 categories, where we also note their category name.

the default controller in real-world only allows 0.47 meters in minimum). This is to show the indispensability of the whole-body behavior. We compare both the teacher and its corresponding student policy using the same policy network structure. 3) Non-hierarchical: a unified policy trained with low-level policy and visuomotor high-level policy jointly in an end-to-end style. This policy takes the observation of our low-level and high-level policies together. It outputs all the target positions of 12 robot joint angles and the target pose of the gripper. We failed in training such a policy, indicating the effectiveness and necessity of the training pipeline of VBC. We design these baselines to provide a valuable analysis of the design of each module and part.

Picking up different objects. We test the picking-up *success rate* on each distinct object for more than 300 episodes and collect the results over every category. During test time, all object heights are randomly set from 0.0m to 0.6m for each trial. As is shown in Tab. I, VBC achieves the best performance on 4/7 categories of objects. It is also interesting that with 3D features, VBC becomes worse at regular objects (compared to *VBC w.o. Shape Feature*), but is much better on irregular objects with complicated shapes, i.e., *long box*, *cup*, *bowl* and *drill*. One possible reason is that, without pre-trained features, the policy targets the object’s center for grasping, which is effective enough on simpler objects yet inapplicable for objects with more complicated shapes. One may notice that the student policy is much worse than the teacher policy, this is because when the robot touches but fails to grasp on the first try, the object will be randomly laid so that its pose will be much harder to grasp within only 150 steps using only visual inputs. In addition, the performance of the student policy of

TABLE I: **Success rates** of VBC compared to baseline method on seven categories of objects, tested in the *simulator*. Each distinct object for more than 300 episodes. The robot starts from a 1.0-meter distance from the table. Every episode ends when the robot successfully picks up the object, the object falls from the table, or the robot fails until 150 steps. With the 3D shape feature, the algorithm is better at handling irregular objects. Detailed descriptions of each method are stated in Section IV-A.

	Policy Type	Ball	Long Box	Square Box	Bottle	Cup	Bowl	Drill
Privileged Teacher	Floating Base	63.25%	20.51%	72.66%	38.07%	69.55%	71.88%	4.17%
	VBC w.o. Shape Feature	96.18%	74.26%	96.80%	82.46%	84.38%	55.84%	73.77%
	VBC (Ours)	89.08%	92.83%	81.87%	76.34%	89.12%	78.14%	84.00%
Visuomotor Student	Non-Hierarchical	0.0%	0.0%	0.0%	0.0%	0.0%	0.0%	0.0%
	Floating Base	42.45%	0.0%	37.36%	8.33%	41.41%	43.57%	3.70%
	VBC (Ours)	55.40%	28.57%	80.00%	56.57%	68.01%	58.96%	53.33%

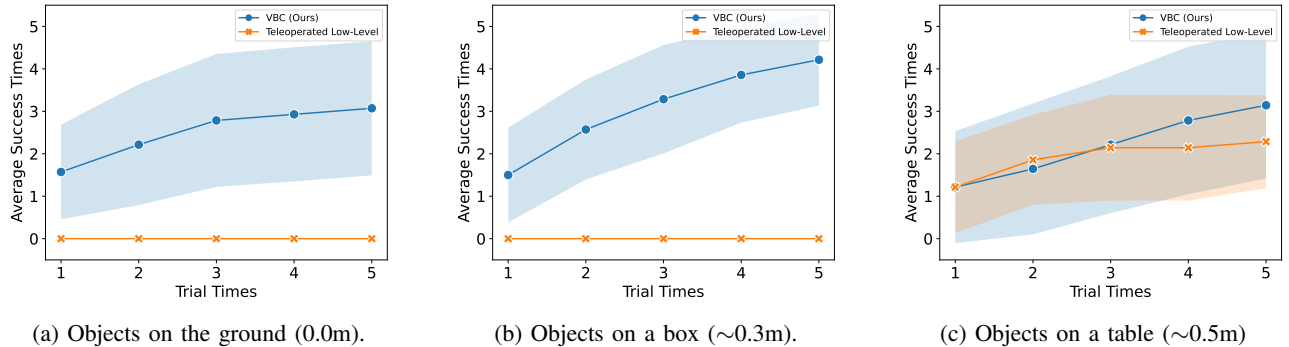


Fig. 11: **Average success times w.r.t. the trial times** of picking up 14 objects at different heights, tested in the *real world*. We allow 5 continuing trial times (including 4 continuous retries, x-axis) during one experiment, i.e., one reset of picking up one specific object. A failure is recorded if the robot attempts more than 5 trails in one reset or if the object falls from a higher surface. For each object and each height, such experiments are conducted 5 times, and therefore we calculate the average success time (y-axis) across these trials, representing the mean number of success times across five trials. It is obvious that **the emergent retrying behavior improves the performance**.

VBC behaves the worst on *long boxes*. This is because without shape features, it is much harder to determine the pose of the object, and some of the initial poses of *long boxes* are extremely hard to grasp for the gripper we used at some height (also as shown in Fig. 10).

Picking up over various heights. We test the mean *success rate* on each object category on a fixed height, where we also list the object with the maximum/minimum success rate on each height. We compare VBC and the floating base baseline on 7 different heights, and illustrate the results in Fig. 10. From the significant improvement of VBC on almost every height, compared to the floating base policy, we highlight the advantage of VBC that is able to achieve flexible whole-body behaviors in achieving high-level tasks.

B. Real-World Experiments

Objects In the real world, we choose 14 objects, including four irregular objects, six common objects, and four regular shapes, shown in Fig. 9. It is worth noting that almost all objects are unseen in the training, i.e., there are no identity objects during real-world experiments.

Evaluation principles and baselines. We deploy the trained visuomotor student policy of VBC as tested in the simulator directly into the real world. In the real world, we test how many times the robot can pick up the assigned object in 5

trials (i.e., the robot is allowed to continuously retry four times when it fails to grasp without resetting), as we find that the robot emerges to have retrying behavior, as will be described below. We choose this as a measurement since we find that the emergent retrying behaviors improve the robustness, reliability, and success rate of finishing a job. We consider it a success when the object is picked more than 0.1m higher than the plane where it is placed and a failure when the robot tries more than five times or the object falls from its surface. Each object is evaluated over three different heights, as stated before, and five resets are permitted for each height. Regarding baselines, we find it hard to build a fair *autonomous* method for comparison, so we compared VBC with the default Unitree base controller (allowing the heights of the arm base to vary from 0.47m to 0.55m) combined with a similar high-level policy trained on stationary legs, in which the robot has no whole-body behaviors but also retains the retrying. We teleoperated the robot to be closed enough to the object before the policy started to grasp. During the test of the real-world experiments, we put the objects at a distance that the cameras mounted on the robot can observe, thus they can be manually annotated using our developed *TrackingSAM* tool. After the annotation, the robot walks by and picks up the objects in a fully *autonomous* way.

Emergent retrying behaviors. It is worth noting that during

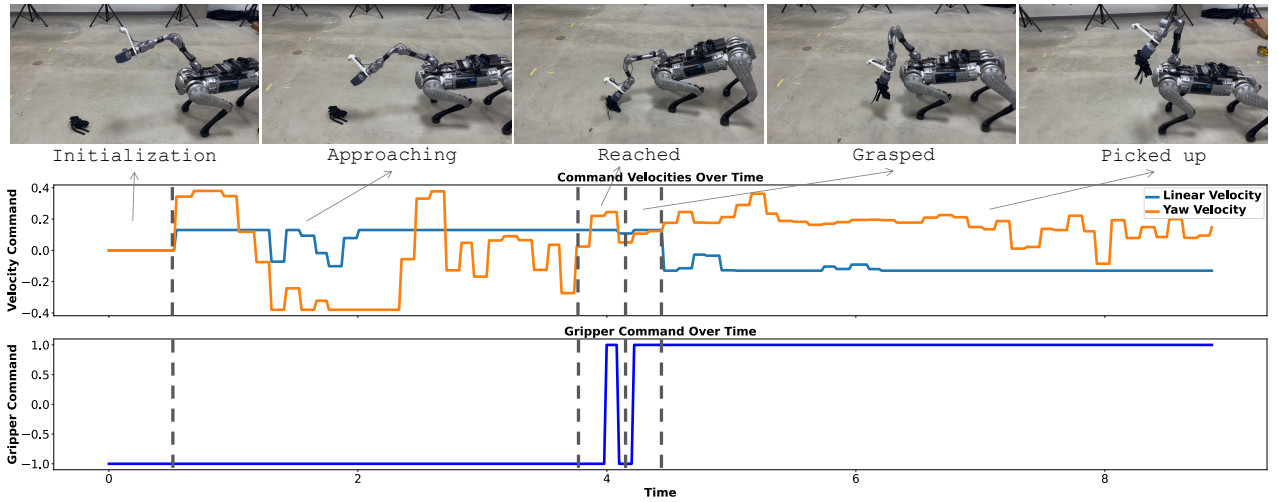


Fig. 12: **Visualization of robot behavior and corresponding commands during the test time.** Particularly, we plot the two kinds of high-level commands given by the high-level policy, as described in Section III-C, i.e., the velocity commands (including the quadruped linear velocity and yaw velocity); along with the gripper command (close or open).

simulation training, the robot emerges to learn a retrying behavior. In other words, when the robot fails to grasp an object, it will automatically retry to grasp without any human intervention. This shows an advantage and a clear difference compared to model-based methods. In our observation, as long as the visual mask is on-track/not-lost, the success rates benefit from 1) the change of the object pose in the early tries; and 2) the movement of the robot body.

Pickup performance. We collect all results and conclude the averaged performance over all objects on each height setting and show in Fig. 11. It is worth noting that our method allows for autonomous retrying behaviors when one pick-up trial fails. Obviously, VBC surpasses the baseline method on all settings. To highlight, the baseline methods fail at 0.0m and 0.3m, as the default controller keeps a fixed robot height, similar to the floating base baseline. Even on the 0.5m setting, where the teleoperated baseline without whole-body behavior is equivalent to a static robotics arm, VBC is generally better. Besides, VBC shows great generalization ability on unseen shapes, thanks to the training strategy and observation design in the training pipeline.

Qualitative analysis. We want to analyze whether the commands sent by the high-level policy are reasonable to call the low-level policy to achieve the task. To this end, we visualize the velocity commands, the gripper command, along with their corresponding robot behavior during the testing time in Figure 12. It appears that there is less gap when deploying our policy trained in the simulator into the real world, which is able to provide the correct commands that show clear phases.

V. CONCLUSIONS, LIMITATIONS AND FUTURE WORKS

In this paper, we proposed a fully autonomous mobile manipulation system based on quadruped robots and a hierarchical training pipeline, Visual Whole-Body Control (VBC). VBC consists of a low-level goal-reaching policy and a high-level task-planning policy, which is trained through re-

inforcement learning and imitation learning. Although we showed great success in picking various objects, we found several failure cases due to the limitations of the system: 1) Compounding error. Our pipeline is hierarchical and requires each module to be coherent and precise to make the robot work well. 2) In-precise depth estimation. The RGBD camera does not reflect a perfect depth estimation, especially on reflective objects. 3) Bad gripper. The gripper of the Unitree Z1 Arm is a beak-like gripper instead of a parallel one, which tends to push objects away and is hard for accurate manipulation. 4) Unstable vision inputs. The tracking SAM that is used to provide the mask of annotated objects, may lose track due to camera deviation and occlusion, or be confused when the selected objects have a similar color to the other things. This is the most common cause leading to failure in our real-world experiments. In our current pipeline, before the robot autonomously picks up objects, we must manually specify the target object in both cameras mounted on the robot. Thanks to the generalizability of trackingSAM, we find that as long as the object is visible to one camera (either the head or the wrist camera), the annotation mask can be propagated to another view for automated picking, and free the robot from being specified in the between of the range of the two cameras, which improves the usability of our system. Since the requirements of annotation and object visibility are totally decoupled from our sim-to-real framework, in the future we can further improve and replace these modules with automated annotation algorithms and a search/exploration module to further improve the automation of the whole system. Future works should also consider upgrading the hardware, like replacing a better gripper and RGBD cameras that provide better depth estimation; and simplify the working pipeline.

ACKNOWLEDGMENTS

We would like to thank Unitree for their technical support. We thank Chengzhe Jia for the great help on 3D modeling. We

also thank Haichuan Che, Jun Wang, Shiqi Yang, and Jialong Li for their kind help in recording demos.

REFERENCES

- [1] Ananye Agarwal, Ashish Kumar, Jitendra Malik, and Deepak Pathak. Legged locomotion in challenging terrains using ego-centric vision. In *Conference on Robot Learning*, pages 403–415. PMLR, 2023.
- [2] Michael Ahn, Anthony Brohan, Noah Brown, Yevgen Chebotar, Omar Cortes, Byron David, Chelsea Finn, Chuyuan Fu, Keerthana Gopalakrishnan, Karol Hausman, et al. Do as i can, not as i say: Grounding language in robotic affordances. *arXiv preprint arXiv:2204.01691*, 2022.
- [3] Rika Antonova, Akshara Rai, and Christopher G Atkeson. Deep kernels for optimizing locomotion controllers. In *Conference on Robot Learning*, pages 47–56. PMLR, 2017.
- [4] Elena Arcari, Maria Vittoria Minniti, Anna Scampicchio, Andrea Carron, Farbod Farshidian, Marco Hutter, and Melanie N Zeilinger. Bayesian multi-task learning mpc for robotic mobile manipulation. *IEEE Robotics and Automation Letters*, 2023.
- [5] C Dario Bellicoso, Koen Krämer, Markus Stäuble, Dhionis Sako, Fabian Jenelten, Marko Bjelonic, and Marco Hutter. Alma-articulated locomotion and manipulation for a torque-controllable robot. In *2019 International conference on robotics and automation (ICRA)*, pages 8477–8483. IEEE, 2019.
- [6] Dominik Belter, Przemysław Łabcki, and Piotr Skrzypczyński. Estimating terrain elevation maps from sparse and uncertain multi-sensor data. In *2012 IEEE International Conference on Robotics and Biomimetics (ROBIO)*, pages 715–722. IEEE, 2012.
- [7] Gerardo Bledt, Matthew J Powell, Benjamin Katz, Jared Di Carlo, Patrick M Wensing, and Sangbae Kim. Mit cheetah 3: Design and control of a robust, dynamic quadruped robot. In *2018 IEEE/RSJ International Conference on Intelligent Robots and Systems (IROS)*, pages 2245–2252. IEEE, 2018.
- [8] Michael Bloesch, Sammy Omari, Marco Hutter, and Roland Siegwart. Robust visual inertial odometry using a direct ekf-based approach. In *2015 IEEE/RSJ international conference on intelligent robots and systems (IROS)*, pages 298–304. IEEE, 2015.
- [9] Anthony Brohan, Noah Brown, Justice Carbajal, Yevgen Chebotar, Joseph Dabis, Chelsea Finn, Keerthana Gopalakrishnan, Karol Hausman, Alex Herzog, Jasmine Hsu, et al. Rt-1: Robotics transformer for real-world control at scale. *arXiv preprint arXiv:2212.06817*, 2022.
- [10] Russell Buchanan, Marco Camurri, Frank Dellaert, and Maurice Fallon. Learning inertial odometry for dynamic legged robot state estimation. In *Conference on robot learning*, pages 1575–1584. PMLR, 2022.
- [11] Berk Calli, Arjun Singh, James Bruce, Aaron Walsman, Kurt Konolige, Siddhartha Srinivasa, Pieter Abbeel, and Aaron M Dollar. Yale-cmu-berkeley dataset for robotic manipulation research. *The International Journal of Robotics Research*, 36(3):261–268, 2017.
- [12] Xuxin Cheng, Ashish Kumar, and Deepak Pathak. Legs as manipulator: Pushing quadrupedal agility beyond locomotion. In *2023 IEEE International Conference on Robotics and Automation (ICRA)*, 2023.
- [13] Xuxin Cheng, Kexin Shi, Ananye Agarwal, and Deepak Pathak. Extreme parkour with legged robots. *arXiv preprint arXiv:2309.14341*, 2023.
- [14] Erwin Coumans and Yunfei Bai. Pybullet, a python module for physics simulation for games, robotics and machine learning. <http://pybullet.org>, 2016–2021.
- [15] Helei Duan, Bikram Pandit, Mohitvishnu S Gadde, Bart Jaap van Marum, Jeremy Dao, Chanh Kim, and Alan Fern. Learning vision-based bipedal locomotion for challenging terrain. *arXiv preprint arXiv:2309.14594*, 2023.
- [16] Alejandro Escontrela, Xue Bin Peng, Wenhao Yu, Tingnan Zhang, Atıl İscen, Ken Goldberg, and Pieter Abbeel. Adversarial motion priors make good substitutes for complex reward functions. In *2022 IEEE/RSJ International Conference on Intelligent Robots and Systems (IROS)*, pages 25–32. IEEE, 2022.
- [17] Péter Fankhauser, Michael Bloesch, Christian Gehring, Marco Hutter, and Roland Siegwart. Robot-centric elevation mapping with uncertainty estimates. In *Mobile Service Robotics*, pages 433–440. World Scientific, 2014.
- [18] Péter Fankhauser, Michael Bloesch, and Marco Hutter. Probabilistic terrain mapping for mobile robots with uncertain localization. *IEEE Robotics and Automation Letters*, 3(4):3019–3026, 2018.
- [19] Siyuan Feng, Eric Whitman, X Xinjilefu, and Christopher G Atkeson. Optimization based full body control for the atlas robot. In *2014 IEEE-RAS International Conference on Humanoid Robots*, pages 120–127. IEEE, 2014.
- [20] Henrique Ferrolho, Vladimir Ivan, Wolfgang Merkt, Ioannis Havoutis, and Sethu Vijayakumar. Roloma: Robust locomotion for quadruped robots with arms. *Autonomous Robots*, 47(8):1463–1481, 2023.
- [21] Zipeng Fu, Ashish Kumar, Ananye Agarwal, Haozhi Qi, Jitendra Malik, and Deepak Pathak. Coupling vision and proprioception for navigation of legged robots. In *Proceedings of the IEEE/CVF Conference on Computer Vision and Pattern Recognition*, pages 17273–17283, 2022.
- [22] Zipeng Fu, Xuxin Cheng, and Deepak Pathak. Deep whole-body control: learning a unified policy for manipulation and locomotion. In *Conference on Robot Learning*, pages 138–149. PMLR, 2023.
- [23] Zipeng Fu, Tony Z Zhao, and Chelsea Finn. Mobile aloha: Learning bimanual mobile manipulation with low-cost whole-body teleoperation. *arXiv preprint arXiv:2401.02117*, 2024.
- [24] Yuni Fuchioka, Zhaoming Xie, and Michiel Van de Panne. Opt-mimic: Imitation of optimized trajectories for dynamic quadruped behaviors. In *2023 IEEE International Conference on Robotics and Automation (ICRA)*, pages 5092–5098. IEEE, 2023.
- [25] Caelan Reed Garrett, Tomás Lozano-Pérez, and Leslie Pack Kaelbling. Pddlstream: Integrating symbolic planners and blackbox samplers via optimistic adaptive planning, 2020.
- [26] Christian Gehring, Stelian Coros, Marco Hutter, Carmine Dario Bellicoso, Huub Heijnen, Remo Diethelm, Michael Bloesch, Péter Fankhauser, Jemin Hwangbo, Mark Hoepfner, et al. Practice makes perfect: An optimization-based approach to controlling agile motions for a quadruped robot. *IEEE Robotics & Automation Magazine*, 23(1):34–43, 2016.
- [27] Jiayuan Gu, Devendra Singh Chaplot, Hao Su, and Jitendra Malik. Multi-skill mobile manipulation for object rearrangement. In *The Eleventh International Conference on Learning Representations*, 2023. URL https://openreview.net/forum?id=Z3ICIM_bzvP.
- [28] Danijar Hafner, Jurgis Pasukonis, Jimmy Ba, and Timothy Lillicrap. Mastering diverse domains through world models, 2023.
- [29] Nicklas Hansen, Hao Su, and Xiaolong Wang. Td-mpc2: Scalable, robust world models for continuous control, 2023.
- [30] Tairan He, Yuge Zhang, Kan Ren, Minghuan Liu, Che Wang, Weinan Zhang, Yuqing Yang, and Dongsheng Li. Reinforcement learning with automated auxiliary loss search. *Advances in Neural Information Processing Systems*, 35:1820–1834, 2022.
- [31] Marco Hutter, Christian Gehring, Dominic Jud, Andreas Lauber, C Dario Bellicoso, Vassilios Tsounis, Jemin Hwangbo, Karen Bodie, Peter Fankhauser, Michael Bloesch, et al. Anymal-

- a highly mobile and dynamic quadrupedal robot. In *2016 IEEE/RSJ international conference on intelligent robots and systems (IROS)*, pages 38–44. IEEE, 2016.
- [32] Seunghun Jeon, Moonkyu Jung, Suyoung Choi, Beomjoon Kim, and Jemin Hwangbo. Learning whole-body manipulation for quadrupedal robot. *IEEE Robotics and Automation Letters*, 9(1):699–706, 2023.
 - [33] Sunwoo Kim, Maks Sorokin, Jehee Lee, and Sehoon Ha. Human motion control of quadrupedal robots using deep reinforcement learning. In *Proceedings of Robotics: Science and Systems*, New York, USA, June 2022.
 - [34] Alexander Kirillov, Eric Mintun, Nikhila Ravi, Hanzi Mao, Chloe Rolland, Laura Gustafson, Tete Xiao, Spencer Whitehead, Alexander C Berg, Wan-Yen Lo, et al. Segment anything. *arXiv preprint arXiv:2304.02643*, 2023.
 - [35] Alexander Kleiner and Christian Dornhege. Real-time localization and elevation mapping within urban search and rescue scenarios. *Journal of Field Robotics*, 24(8-9):723–745, 2007.
 - [36] Ashish Kumar, Zipeng Fu, Deepak Pathak, and Jitendra Malik. Rma: Rapid motor adaptation for legged robots. *arXiv preprint arXiv:2107.04034*, 2021.
 - [37] Ashish Kumar, Zhongyu Li, Jun Zeng, Deepak Pathak, Koushil Sreenath, and Jitendra Malik. Adapting rapid motor adaptation for bipedal robots. In *2022 IEEE/RSJ International Conference on Intelligent Robots and Systems (IROS)*, pages 1161–1168. IEEE, 2022.
 - [38] K. Niranjan Kumar, Irfan Essa, and Sehoon Ha. Cascaded compositional residual learning for complex interactive behaviors. *IEEE Robotics and Automation Letters*, 8(8):4601–4608, 2023. doi: 10.1109/LRA.2023.3286171.
 - [39] K. Niranjan Kumar, Irfan Essa, and Sehoon Ha. Words into action: Learning diverse humanoid robot behaviors using language guided iterative motion refinement, 2023.
 - [40] In-So Kweon and Takeo Kanade. High-resolution terrain map from multiple sensor data. *IEEE Transactions on Pattern Analysis and Machine Intelligence*, 14(2):278–292, 1992.
 - [41] Joonho Lee, Jemin Hwangbo, Lorenz Wellhausen, Vladlen Koltun, and Marco Hutter. Learning quadrupedal locomotion over challenging terrain. *Science robotics*, 5(47):eabc5986, 2020.
 - [42] Thomas Lew, Sumeet Singh, Mario Prats, Jeffrey Bingham, Jonathan Weisz, Benjie Holson, Xiaohan Zhang, Vikas Sindhwani, Yao Lu, Fei Xia, Peng Xu, Tingnan Zhang, Jie Tan, and Montserrat Gonzalez. Robotic table wiping via reinforcement learning and whole-body trajectory optimization, 2022.
 - [43] Chenhao Li, Marin Vlastelica, Sebastian Blaes, Jonas Frey, Felix Grimminger, and Georg Martius. Learning agile skills via adversarial imitation of rough partial demonstrations. In *Conference on Robot Learning*, pages 342–352. PMLR, 2023.
 - [44] Zhongyu Li, Xuxin Cheng, Xue Bin Peng, Pieter Abbeel, Sergey Levine, Glen Berseth, and Koushil Sreenath. Reinforcement learning for robust parameterized locomotion control of bipedal robots. In *2021 IEEE International Conference on Robotics and Automation (ICRA)*, pages 2811–2817. IEEE, 2021.
 - [45] Minghuan Liu, Tairan He, Minkai Xu, and Weinan Zhang. Energy-based imitation learning. *arXiv preprint arXiv:2004.09395*, 2020.
 - [46] Yuntao Ma, Farbod Farshidian, Takahiro Miki, Joonho Lee, and Marco Hutter. Combining learning-based locomotion policy with model-based manipulation for legged mobile manipulators. *IEEE Robotics and Automation Letters*, 7(2):2377–2384, 2022.
 - [47] Viktor Makoviychuk, Lukasz Wawrzyniak, Yunrong Guo, Michelle Lu, Kier Storey, Miles Macklin, David Hoeller, Nikita Rudin, Arthur Allshire, Ankur Handa, et al. Isaac gym: High performance gpu-based physics simulation for robot learning. *arXiv preprint arXiv:2108.10470*, 2021.
 - [48] Gabriel B Margolis and Pulkit Agrawal. Walk these ways: Tuning robot control for generalization with multiplicity of behavior. In *Conference on Robot Learning*, pages 22–31. PMLR, 2023.
 - [49] Takahiro Miki, Joonho Lee, Jemin Hwangbo, Lorenz Wellhausen, Vladlen Koltun, and Marco Hutter. Learning robust perceptive locomotion for quadrupedal robots in the wild. *Science Robotics*, 7(62):eabk2822, 2022.
 - [50] Hirofumi Miura and Isao Shimoyama. Dynamic walk of a biped. *The International Journal of Robotics Research*, 3(2): 60–74, 1984.
 - [51] Chuong Nguyen, Lingfan Bao, and Quan Nguyen. Continuous jumping for legged robots on stepping stones via trajectory optimization and model predictive control. In *2022 IEEE 61st Conference on Decision and Control (CDC)*, pages 93–99. IEEE, 2022.
 - [52] Quan Nguyen, Ayush Agrawal, Xingye Da, William C Martin, Hartmut Geyer, Jessy W Grizzle, and Koushil Sreenath. Dynamic walking on randomly-varying discrete terrain with one-step preview. In *Robotics: Science and Systems*, volume 2, pages 384–99, 2017.
 - [53] Quan Nguyen, Matthew J Powell, Benjamin Katz, Jared Di Carlo, and Sangbae Kim. Optimized jumping on the mit cheetah 3 robot. In *2019 International Conference on Robotics and Automation (ICRA)*, pages 7448–7454. IEEE, 2019.
 - [54] Xue Bin Peng, Erwin Coumans, Tingnan Zhang, Tsang-Wei Lee, Jie Tan, and Sergey Levine. Learning agile robotic locomotion skills by imitating animals. *arXiv preprint arXiv:2004.00784*, 2020.
 - [55] Charles R Qi, Hao Su, Kaichun Mo, and Leonidas J Guibas. Pointnet: Deep learning on point sets for 3d classification and segmentation. In *Proceedings of the IEEE conference on computer vision and pattern recognition*, pages 652–660, 2017.
 - [56] Rizhao Qiu. *Towards real-time robotics perception with continual adaptation*. PhD thesis, University of Illinois at Urbana-Champaign, 2023.
 - [57] Stéphane Ross, Geoffrey Gordon, and Drew Bagnell. A reduction of imitation learning and structured prediction to no-regret online learning. In *Proceedings of the fourteenth international conference on artificial intelligence and statistics*, pages 627–635. JMLR Workshop and Conference Proceedings, 2011.
 - [58] Nikita Rudin, David Hoeller, Philipp Reist, and Marco Hutter. Learning to walk in minutes using massively parallel deep reinforcement learning. In *Conference on Robot Learning*, pages 91–100. PMLR, 2022.
 - [59] Nur Muhammad Mahi Shafiullah, Anant Rai, Haritheja Etukuru, Yiqian Liu, Ishan Misra, Soumith Chintala, and Lerrel Pinto. On bringing robots home. *arXiv preprint arXiv:2311.16098*, 2023.
 - [60] Jean-Pierre Sleiman, Farbod Farshidian, and Marco Hutter. Versatile multicontact planning and control for legged locomotion. *Science Robotics*, 8(81):eadg5014, 2023.
 - [61] Koushil Sreenath, Hae-Won Park, Ioannis Poulakakis, and Jessy W Grizzle. A compliant hybrid zero dynamics controller for stable, efficient and fast bipedal walking on mabel. *The International Journal of Robotics Research*, 30(9):1170–1193, 2011.
 - [62] Siddharth Srivastava, Eugene Fang, Lorenzo Riano, Rohan Chitnis, Stuart Russell, and Pieter Abbeel. Combined task and motion planning through an extensible planner-independent interface layer. In *2014 IEEE International Conference on Robotics and Automation (ICRA)*, pages 639–646, 2014. doi: 10.1109/ICRA.2014.6906922.
 - [63] Charles Sun, Jędrzej Orbik, Coline Manon Devin, Brian H Yang, Abhishek Gupta, Glen Berseth, and Sergey Levine. Fully autonomous real-world reinforcement learning with applications to mobile manipulation. In *Conference on Robot Learning*, pages 308–319. PMLR, 2022.
 - [64] Yikai Wang, Zheyuan Jiang, and Jianyu Chen. Amp in the wild:

- Learning robust, agile, natural legged locomotion skills. *arXiv preprint arXiv:2304.10888*, 2023.
- [65] David Wisth, Marco Camurri, and Maurice Fallon. Robust legged robot state estimation using factor graph optimization. *IEEE Robotics and Automation Letters*, 4(4):4507–4514, 2019.
 - [66] David Wisth, Marco Camurri, and Maurice Fallon. Vilens: Visual, inertial, lidar, and leg odometry for all-terrain legged robots. *IEEE Transactions on Robotics*, 39(1):309–326, 2022.
 - [67] Wouter J Wolfslag, Christopher McGreavy, Guiyang Xin, Carlo Tiseo, Sethu Vijayakumar, and Zhibin Li. Optimisation of body-ground contact for augmenting the whole-body locomanipulation of quadruped robots. In *2020 IEEE/RSJ International Conference on Intelligent Robots and Systems (IROS)*, pages 3694–3701. IEEE, 2020.
 - [68] Josiah Wong, Albert Tung, Andrey Kurenkov, Ajay Mandlekar, Li Fei-Fei, Silvio Savarese, and Roberto Martín-Martín. Error-aware imitation learning from teleoperation data for mobile manipulation. In *Conference on Robot Learning*, pages 1367–1378. PMLR, 2022.
 - [69] Fei Xia, Chengshu Li, Roberto Martín-Martín, Or Litany, Alexander Toshev, and Silvio Savarese. Relmogen: Leveraging motion generation in reinforcement learning for mobile manipulation, 2021.
 - [70] Guowei Xu, Ruijie Zheng, Yongyuan Liang, Xiyao Wang, Zhecheng Yuan, Tianying Ji, Yu Luo, Xiaoyu Liu, Jiabin Yuan, Pu Hua, Shuzhen Li, Yanjie Ze, Hal Daumé III au2, Furong Huang, and Huazhe Xu. Dm: Mastering visual reinforcement learning through dormant ratio minimization, 2023.
 - [71] Ruihan Yang, Zhuoqun Chen, Jianhan Ma, Chongyi Zheng, Yiyu Chen, Quan Nguyen, and Xiaolong Wang. Generalized animal imitator: Agile locomotion with versatile motion prior. *arXiv preprint arXiv:2310.01408*, 2023.
 - [72] Ruihan Yang, Yejin Kim, Aniruddha Kembhavi, Xiaolong Wang, and Kiana Ehsani. Harmonic mobile manipulation. *arXiv preprint arXiv:2312.06639*, 2023.
 - [73] Ruihan Yang, Ge Yang, and Xiaolong Wang. Neural volumetric memory for visual locomotion control. In *Proceedings of the IEEE/CVF Conference on Computer Vision and Pattern Recognition*, pages 1430–1440, 2023.
 - [74] Shuo Yang, Hans Kumar, Zhaoyuan Gu, Xiangyuan Zhang, Matthew Travers, and Howie Choset. State estimation for legged robots using contact-centric leg odometry. *arXiv preprint arXiv:1911.05176*, 2019.
 - [75] Taozheng Yang, Ya Jing, Hongtao Wu, Jiafeng Xu, Kuankuan Sima, Guangzeng Chen, Qie Sima, and Tao Kong. Moma-force: Visual-force imitation for real-world mobile manipulation. In *2023 IEEE/RSJ International Conference on Intelligent Robots and Systems (IROS)*, pages 6847–6852. IEEE, 2023.
 - [76] Zongxin Yang, Yunchao Wei, and Yi Yang. Associating objects with transformers for video object segmentation. *Advances in Neural Information Processing Systems*, 34:2491–2502, 2021.
 - [77] Denis Yarats, Rob Fergus, Alessandro Lazaric, and Lerrel Pinto. Mastering visual continuous control: Improved data-augmented reinforcement learning. In *International Conference on Learning Representations*, 2022. URL https://openreview.net/forum?id=_SJ-_yyes8.
 - [78] Naoki Yokoyama, Alex Clegg, Joanne Truong, Eric Undersander, Tsung-Yen Yang, Sergio Arnaud, Sehoon Ha, Dhruv Batra, and Akshara Rai. Asc: Adaptive skill coordination for robotic mobile manipulation, 2023.
 - [79] Naoki Yokoyama, Alexander William Clegg, Eric Undersander, Sehoon Ha, Dhruv Batra, and Akshara Rai. Adaptive skill coordination for robotic mobile manipulation. *arXiv preprint arXiv:2304.00410*, 2023.
 - [80] Wenhao Yu, Deepali Jain, Alejandro Escontrela, Atil Iscen, Peng Xu, Erwin Coumans, Sehoon Ha, Jie Tan, and Tingnan Zhang. Visual-locomotion: Learning to walk on complex terrains with vision. In *5th Annual Conference on Robot Learning*, 2021.
 - [81] Jiazhao Zhang, Nandiraju Gireesh, Jilong Wang, Xiaomeng Fang, Chaoyi Xu, Weiguang Chen, Liu Dai, and He Wang. Gamma: Graspability-aware mobile manipulation policy learning based on online grasping pose fusion. *arXiv preprint arXiv:2309.15459*, 2023.
 - [82] Ziwen Zhuang, Zipeng Fu, Jianren Wang, Christopher Atkeson, Soeren Schwertfeger, Chelsea Finn, and Hang Zhao. Robot parkour learning. *arXiv preprint arXiv:2309.05665*, 2023.
 - [83] Simon Zimmermann, Roi Poranne, and Stelian Coros. Go fetch!-dynamic grasps using boston dynamics spot with external robotic arm. In *2021 IEEE International Conference on Robotics and Automation (ICRA)*, pages 4488–4494. IEEE, 2021.

Visual Whole-Body Control for Legged Loco-Manipulation

Appendix

I. NOTATIONS AND BACKGROUND

A. Reinforcement Learning

Reinforcement learning (RL) is usually formulated as a γ -discounted infinite horizon Markov decision process (MDP) $\mathcal{M} = \langle \mathcal{S}, \mathcal{A}, \mathcal{T}, \rho_0, r, \gamma \rangle$, where \mathcal{S} is the state space, \mathcal{A} is the action space, $\mathcal{T} : \mathcal{S} \times \mathcal{A} \rightarrow \mathcal{S}$ is the environment dynamics function, $\rho_0 : \mathcal{S} \rightarrow [0, 1]$ is the initial state distribution, $r(s, a) : \mathcal{S} \times \mathcal{A} \rightarrow \mathbb{R}$ is the reward function, and $\gamma \in [0, 1]$ is the discount factor. The goal of RL is to train an agent with policy $\pi(a|s) : \mathcal{S} \rightarrow \mathcal{A}$ to maximize the accumulated reward $R = \sum_t \gamma^t r(s_t, a_t)$.

B. Proximal Policy Optimization

Proximal policy optimization (PPO) is one of the popular algorithms that solve RL problems. The basic idea behind PPO is to maximize a surrogate objective that constrains the size of the policy update. In particular, PPO optimizes the following objective:

$$L^{PPO}(\theta_\pi) = \mathbb{E}_\pi[\min(rA, \text{clip}(r, 1 - \epsilon, 1 + \epsilon)A)], \quad (5)$$

where $r = \frac{\pi(a|s)}{\pi_{old}(a|s)}$ defines the probability ratio of the current policy and the old policy at the last optimization step, $A(s, a)$ is the advantage function, and θ_π is the parameter of the policy π .

C. Imitation Learning

In general, imitation learning (IL) [57, 45] studies the task of learning from expert demonstrations. In this work, instead of learning from offline expert data, we refer to an online IL method, dataset aggregation (DAgger) [57] such that we request an online expert to provide the demonstrated action. Formally, the goal is to train a student policy $\hat{\pi}$ minimizing the action distance between the expert policy π_E under its encountered states:

$$\hat{\pi} = \arg \min_{\pi \in \Pi} \mathbb{E}_{s \sim d_\pi} [\ell(s, \pi)]. \quad (6)$$

In this paper, ℓ is the mean square error in practice.

D. Whole-Body Control

Whole-body control in robotics refers to controlling a mobile manipulator with the function of locomotion and manipulation by one unified framework. In this work, we consider a system that contains a quadruped robot combined with a 6-DoF robot arm, each of which has an underlying PD controller, and we use a learned policy to generate control signals and feed them to the controller given 1) the robot states and 2) commands.

In detail, the policy used for controlling the quadruped robot is driven by external commands, such as the base velocity command; and the arm is controlled by a PD controller driven by the $\text{SE}(3)$ end-effector position-orientation command.

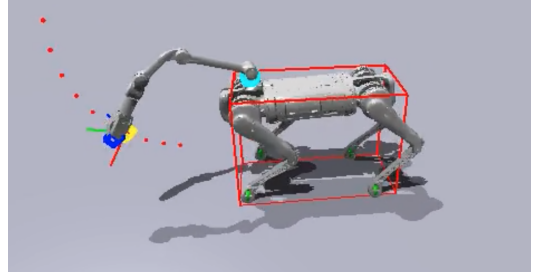


Fig. 13: A screenshot of low-level training, where the robot is required to track the given velocity commands (linear and yaw) and the end-effector pose.

Simulation We use the GPU-based Isaac Gym simulator [47] where we train 4096 environments in parallel.

II. TRAINING DETAILS

A. Low-Level Training

Low-level commands sampling. To train a robust low-level controller for goal-reaching, we should sample and track various goals (i.e., base velocity commands and end-effector commands) as possible. As for the base velocity commands, we uniformly sample the linear velocity from a range of $[-0.6, 0.6]$, and the angular velocity from a range of $[1.0, 1.0]$. Regarding the end-effector, we employ a height-invariant coordinate system originating at the robot's base. Such a design ensures the sampled trajectories are always on a sphere, guaranteeing the consistency of these samples; besides, it prevents the sampled goals from being affected by the quadruped robot's height. In particular, we interpolate the end-effector goal command \mathbf{p}^{cmd} between the current end-effector position \mathbf{p} and a randomly selected end-effector position \mathbf{p}^{end} , at intervals of T_{traj} seconds:

$$\mathbf{p}_t^{\text{cmd}} = \frac{t}{T_{\text{traj}}} \mathbf{p} + \left(1 - \frac{t}{T_{\text{traj}}}\right) \mathbf{p}^{\text{end}}, t \in [0, T_{\text{traj}}].$$

\mathbf{p}^{end} is resampled in a fixed timestep or if any $\mathbf{p}_t^{\text{cmd}}$ leads to self-collision or collision with the ground, similar to the linear and yaw velocity commands $v_{\text{lin}}^{\text{cmd}}, \omega_{\text{yaw}}^{\text{cmd}}$ that are uniformly sampled from a given range. Fig. 13 shows a screenshot of the low-level training, where the robot is required to track the given velocity commands and the end-effector pose.

Regularized online adaptation for sim-to-real transfer. We take the training paradigm of Regularized Online Adaptation (ROA) [22, 12, 32] in the RL training to help decrease the realizability gap when deploying our system into the real world. As illustrated in Fig. 3, we have an encoder μ that takes the privileged information e such as friction and mass as input and predicts an environment extrinsic latent vector z^μ . Then, the adaptation module ϕ estimates this z^μ only based on

TABLE II: Details of low-level policy.

Definition of Symbols		Reward Function Details for the Low-Level Policy		
Name	Symbol	Name	Definition	Weight
Leg joint positions	\mathbf{q}	Linear velocity tracking	$\phi(v_{b,xy}^* - v_{b,xy})$	1
Leg joint velocities	$\dot{\mathbf{q}}$	Yaw velocity tracking	$\phi(v_{yaw}^* - \omega_b)$	0.5
Leg joint accelerations	$\ddot{\mathbf{q}}$	Angular velocity penalty	$-\ \omega_{b,xy}\ ^2$	0.05
Target leg joint positions	\mathbf{q}^*	Joint torques	$-\ \tau\ ^2$	0.00002
Leg joint torques	τ	Action rate	$-\ \mathbf{q}^*\ ^2$	0.25
Base linear velocity	v_b	Collisions	$-n_{collision}$	0.001
Base angular velocity	ω_b	Feet air time	$\sum_{i=0}^4 (t_{air,i} - 0.5)$	2
Base linear velocity command	v_x^*	Default Joint Position Error	$\exp(-0.05\ \mathbf{q} - \mathbf{q}_{default}\)$	1
Base angular velocity command	v_{yaw}^*	Linear Velocity z	$\ v_{b,z}\ ^2$	-1.5
Number of collisions	n_c	Base Height	$\ h_b - h_{b,target}\ $	-5.0
Feet contact force	\mathbf{f}^{foot}	Swing Phase Tracking (Force)	$\sum_{foot} (1 - C_{foot}^{cmd}(\theta_{cmd}, t)) (1 - \exp(-\ \mathbf{f}^{foot}\ ^2 / \sigma_{cf}))$	-0.2
Feet velocity in Z axis	\mathbf{v}_z^{foot}	Stance Phase Tracking (Velocity)	$\sum_{foot} (C_{foot}^{cmd}(\theta_{cmd}, t)) (1 - \exp(-\ \mathbf{v}_z^{foot}\ ^2 / \sigma_{cv}))$	-0.2
Feet air time	t_{air}			
Timing offsets	θ_{cmd}			
Stepping frequency	f_{cmd}			

recent history low-level observations. The adaptation module ϕ is trained by imitating z^μ online. We can then formulate the loss function of our whole low-level policy w.r.t. policy's parameters $\theta_{\pi^{low}}$, privileged information encoder's parameters θ_μ , and adaptation module's parameters θ_ϕ as:

$$L(\theta_{\pi^{low}}, \theta_\mu, \theta_\phi) = -L^{PPO}(\theta_{\pi^{low}}, \theta_\mu) + \lambda \|z^\mu - \text{sg}[z^\phi]\|_2 + \|\text{sg}[z^\mu] - z^\phi\|_2 \quad (7)$$

where $\text{sg}[\cdot]$ is the gradient stop operator, and λ is the Lagrangian multiplier. We optimize this loss function using the dual gradient descent method, and [22] has identified that such an optimization converges under mild conditions. It is worth noticing that RMA [36] is a special case of ROA, where the Lagrangian multiplier λ is set to be constant zero. The adaptation module ϕ starts training only after convergence of the policy π^{low} and the encoder μ .

Reward functions. The detailed definitions of the low-level reward functions are shown in Tab. II, where we define $\phi = \exp(-\frac{\|x\|^2}{0.25})$ for tracking the desired velocity of the robot. It is worth noting that we introduce the swing phase tracking rewards to help the robot learn trotting, and $C_{foot}^{cmd}(\theta_{cmd}, t)$ computes the desired contact state of each foot from the phase and timing variable, as described in [48].

B. High-Level Training

The privileged teacher policy is trained through RL, specifically, we use PPO for training with designed reward functions. **Reward functions** We put all reward functions along with their weights of training the high-level policies in Tab. III. Except for $r_{progress}$, $r_{completion}$ and $r_{completion}$ that is determined by the task stage, we define a set of assistant rewards to help the algorithm converge faster. Among them, r_{acc} limits the arm joints velocities' change rate; r_{cmd} is designed to encourage the robot to slow its velocity when it is close to the object to be picked., r_{action} helps smooth the output of the high-level policy to prevent it from changing quickly; $r_{ee\text{ orn}}$ and $r_{base\text{ orn}}$ encourages the arm and the robot body to be aimed at the

object; $r_{base\text{ approach}}$ encourages the robot to be close to the object when the robot is far away from the object.

TABLE III: Details of High-Level Rewards, where $\dot{\mathbf{q}}$ denotes arm joint velocities; v_x^* denotes base velocity command; \mathbf{d}_{obj} , \mathbf{d}_{ee} and \mathbf{d}_{base} are the direction from robot body to the object, the direction from end-effector to the object and the direction of the robot body orientation, separately; \mathbf{x}_{obj} and \mathbf{x}_{base} are the position coordinates in world frame of the object and the robot body.

	Definition	Weights
Stage Rewards	$r_{approach}$ (Eq. (2))	0.5
	$r_{progress}$ (Eq. (3))	1.0
	$r_{completion}$ (Eq. (4))	3.5
Assistant Rewards	$r_{acc} = 1 - \exp(-\ \dot{\mathbf{q}}_t - \dot{\mathbf{q}}_{t-1}\)$	-0.001
	$r_{cmd} = -\ v_x^* + 0.25 \exp(-\ v_x^*\)$	1.0
	$r_{action} = 1 - \exp(-\ \mathbf{a}_t - \mathbf{a}_{t-1}\)$	-0.001
	$r_{ee\text{ orn}} = \mathbf{d}_{obj} \cdot \mathbf{d}_{ee} $	-0.05
	$r_{base\text{ orn}} = \cos(\mathbf{d}_{obj}, \mathbf{d}_{base})$	0.25
	$r_{base\text{ approach}} = \mathbf{x}_{obj} - \mathbf{x}_{base} $	0.01

Simulation We use the GPU-based Isaac Gym simulator [47]. As for the teacher, we train 10240 environments in parallel; regarding the student, we only utilize 240 parallel environments as there is a huge GPU memory cost for rendering visual observations. Experiments are trained on a single GPU (we use GTX4090 and GTX3090). On a GTX4090, The teacher policy takes around 36 hours for training, and the student policy consumes around 48 hours.

Additional Training Techniques We design several training techniques with our prior knowledge to help the high-level policy to be well-performed and stable, not only in the simulation, but can also be transferred into the real world. We briefly introduce them in the following:

- 1) Action delay. We add a one-step action delay to cover the inference and execution in the real world.
- 2) Command clip curriculum. We gradually clip the linear velocity command during training, as we find that a large velocity helps accelerate the learning convergence

but a slow velocity highly stabilizes the real world performance.

- 3) Reward curriculum. The command penalty reward r_{cmd} is added after the robot learns well to pick up objects.
- 4) Randomly changes the object position. During training, we take a small probability (10%) to randomly change the object position and pose. This helps the robot to learn the retrying behaviors when it fails during one trial.
- 5) Forcing stop when closing gripper. We forcibly set the velocity command to 0 when the gripper command is closing. This contributes a lot to a stop-then-pick behavior and thus improves the performance.

These training techniques are adopted for both teacher policy and student policy training. When training the student policy, we additionally randomize the camera latency as the policy will never obtain the immediate images at the time it infers, but some pictures that are a few milliseconds before, similar to the real world. We randomize the value by measuring the camera latency of the device we used in our real-world experiments.